

Analysis of a nano-porous multi-layer film for thermal radiation barrier coatings

Kaushik Das · Dimitris C. Lagoudas ·
John D. Whitcomb

Received: 24 June 2011 / Accepted: 1 August 2011 / Published online: 20 September 2011
© The Author(s) 2011. This article is published with open access at Springerlink.com

Abstract A highly reflective thermal radiation barrier coating (TRBC) made of a multi-layer film is studied for high temperature applications. The multi-layer film with a periodic microstructure consisting of cylindrical nano-pores acts a photonic band gap (PBG) crystal. The coating is constructed such that pores are arranged periodically along the in-plane directions and axes of the pores are parallel to the thickness direction. The pore diameter is varied periodically through the thickness to form a multi-layer film of alternating low and high porosities. The primary motivation behind considering this microstructure is that it can be fabricated from aluminum dioxide, which remains stable at high temperatures. The reflectivity of a single layer with uniform porosity is computed by numerically solving Maxwell's equations, by considering both the microstructure explicitly and a homogenized layer to gain insights into the effect of pore size on the reflectivity of the nano-porous layer. Based on the study of the single layer, two microstructures with different arrangements of pores are designed to exploit the effect of microstructure to widen the band gap of the PBG crystal and to increase the reflectivity of the TRBC. Results of numerical simulations reveal that a wider band gap and higher reflectivity can be achieved by making the inter-pore distance of alternate layers of the multi-layer film comparable to the wavelength of the incident thermal radiation. A TRBC, which is made of a microstructure with a wider band gap and has increased reflectivity, will reflect

a greater amount of incident heat energy over a wider range of frequencies.

Keywords Thermal radiation barrier coating · Multi-layer film · Anodic aluminum dioxide · Nanostructured material

Introduction

A thermal radiation barrier coating (TRBC) made of a highly reflective multi-layer film is studied for high temperature applications. The multi-layer film has a periodic microstructure, which consists of cylindrical nano-pores and acts as a photonic band gap (PBG) crystal. A PBG crystal is a periodic microstructure designed to affect the propagation of electromagnetic waves. The dielectric constant varies periodically through the microstructure and blocks transmission of electromagnetic waves of a certain frequency range, which is known as a band gap (Joannopoulos et al. 1995; Yablonovitch 2001). A film made of a PBG crystal has higher reflectivity for electromagnetic waves with frequencies within the PBG crystal's band gap (Cornelius and Dowling 1999). Different PBG crystals have been extensively studied numerically and experimentally (Yablonovitch et al. 1991; Sözüer et al. 1992; Ho et al. 1994; Sahrai et al. 2010). Most of the PBG crystals used in electronic devices such as waveguides and filters are based on semiconductor materials because of their compatibility with the microelectronic manufacturing processes (Mekis et al. 1996; Winn et al. 1998; Painter et al. 1999; Noda et al. 2002). Apart from their use in the electronic industry, films of PBG crystals made of materials that are stable at high temperature are used in aerospace industry as highly reflective TRBCs to reflect

K. Das (✉) · D. C. Lagoudas · J. D. Whitcomb
Department of Aerospace Engineering,
Texas A&M University, College Station,
TX 77843, USA
e-mail: k.das@tamu.edu

thermal radiation in high temperature applications (Siegel and Spuckler 1998; Nicholls et al. 2002; Wolfe et al. 2005; Wang et al. 2006; Shklover et al. 2008; Huang 2009).

A typical thermal barrier coating protects structures, such as the hyper-sonic airplanes, combustor liners, turbine vanes and blades against heat convection from high temperature flows (Siegel and Spuckler 1998). Studies have shown that radiative heat flux is significant compared to the convective heat flux in flows with temperature greater than 1,000 K (Rolin et al. 1981; Kim and Baek 1996; Chen 1997; Krishnaprakas et al. 2000; Ko and Anand 2008). The wavelength of radiation emitted by the hot fluid depends on the type and the temperature of the fluid. In the case of a black body, the wavelength for which the intensity of the emitted radiation is high varies from 0.5 to 4 μm for a temperature range from 1,000 to 1,500 K (Modest 2003). Therefore, a thermal barrier coating should have increased reflectivity for wavelength range of ~ 0.5 to ~ 4 μm . Ceramic materials usually used for thermal barrier coatings are not a good reflector of thermal radiation in this wavelength range (Siegel and Spuckler 1998). Thus, a film of PBG crystals having high reflectivity for wavelengths of 1–4 μm would act as a TRBC, which could be applied on a typical thermal barrier coating to increase its reflectivity. A film made of alternate layers of yttria stabilized zirconia (YSZ) and aluminum oxide (Al_2O_3) has been proposed for application as a TRBC (Kelly et al. 2006). Another TRBC made of layers of ceramic and metal has been proposed by Huang (2009).

Recently, a highly ordered three dimensional (3-D) microstructure was fabricated using Al_2O_3 (Lee et al. 2006). The microstructure consists of cylindrical pores such that axes of pores are parallel to each other and pores are arranged periodically along a plane perpendicular to the axes of cylindrical pores. The diameter of a pore varied periodically to form a multi-layer microstructure of alternating low and high porosities. Thus, the microstructure can be considered as a stack of alternate layers of high and low effective dielectric constants. Due to this periodic variation of the effective dielectric constant in the transverse direction to the layers, the microstructure can be used as a PBG crystal with a band gap for waves propagating along the transverse direction. A film of the PBG crystal made of Al_2O_3 would be suitable as a TRBC due to its microstructural stability at high temperature ($>1,500$ K), high melting point (2,345 K) and low thermal conductivity (<18 W/mK) (Yang et al. 2003).

The task of studying a highly reflective TRBC made of a PBG crystal is twofold. The first task is to calculate band gaps of the PBG crystal. The electromagnetic field inside a periodic microstructure can be expressed in the form of Bloch waves (Joannopoulos et al. 1995) so that only a unit cell analysis of the microstructure is necessary to determine

band gaps by applying appropriate periodic boundary conditions. However, except for a few simple unit cells, band gaps cannot be obtained analytically and numerical methods, such as the plane-wave expansion method (Leung and Liu 1990; Datta et al. 1992; Liu and Liu 1999; Guo and Albin 2003), are required. The second task is to estimate the reflectivity of the TRBC. This requires consideration of a 3-D domain consisting of at least one unit cell of the microstructure along the in-plane directions and the full thickness of the multi-layer TRBC (Prather et al. 2009). Numerical methods, such as the finite difference time domain method (Taflove and Hagness 2000), are often employed because the reflectivity of a TRBC with complex 3-D microstructure cannot be obtained analytically.

It has been found from the literature study that the reflectivity of a multi-layer TRBC of a nano-porous microstructure, similar to the one made of Al_2O_3 (Lee et al. 2006), and the band gap of the microstructure have not been studied before. In the current work, a TRBC made of nano-porous multi-layer microstructure is studied. Two different microstructures with different arrangement of pores are examined to study the possibility of exploiting the effect of the microstructure to increase the band gap width and the reflectivity. A TRBC, which is made of a microstructure with a wider band gap and has increased reflectivity, will reflect greater amount of heat energy incident on the structure with a wider range of frequencies from the outside hot environment. Parametric studies on the effect of the size and arrangement of pores on the band gap of the microstructure and the reflectivity of the multi-layer TRBC are presented. Results obtained by considering the microstructure explicitly are compared to those obtained by considering a homogenized microstructure to examine the effect of the size and arrangement of pores. The effective dielectric constants of homogenized microstructures are estimated from the Maxwell-Garnett method (Garnett 1904).

The organization of the present article is the following: in the next section, the general equations used for computation of the reflectivity of a multi-layer TRBC and the band gap of a multi-layer microstructure are presented followed by results and discussions. Conclusions are summarized in the last section.

Mathematical model

Computation of reflectivity of a multi-layer TRBC

In this section, the governing equations of electromagnetism for computation of the reflectivity of a multi-layer TRBC are presented. A schematic of the problem domain and unit vectors \mathbf{e}_i ($i = 1, 2$ or 3) along the Cartesian coordinate directions are shown in Fig. 1. The domain

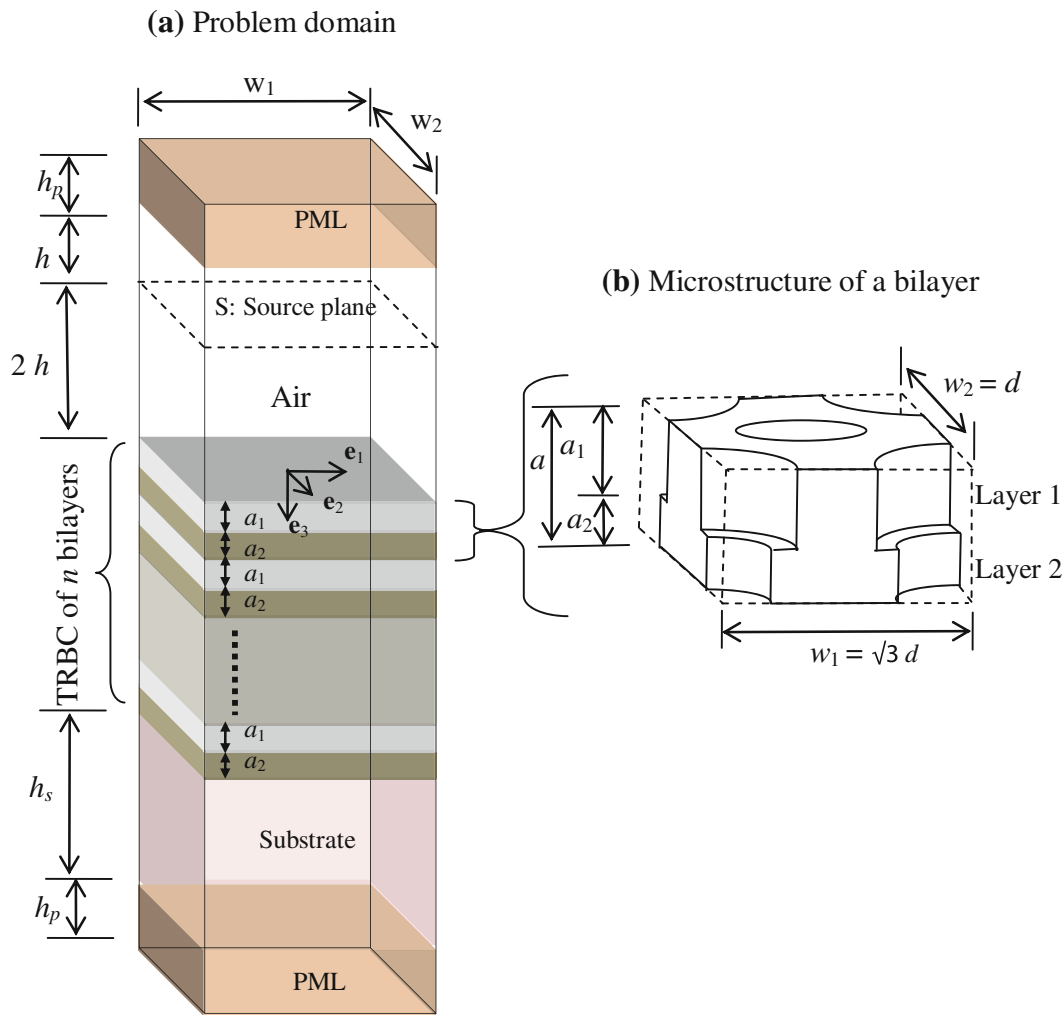


Fig. 1 A schematic of the problem domain consisting of a TRBC, a substrate, an air region, and two perfectly matched layers (PMLs)

consists of a TRBC of n bilayers, a substrate layer below and air above the TRBC. The substrate layer represents a solid ceramic thermal barrier coating. The problem domain is truncated in the positive and the negative \mathbf{e}_3 directions by layers of an artificial absorbing material known as the perfectly matched layer (PML) (Berenger 1994; Oskooi et al. 2008). Use of PMLs, which completely absorb electromagnetic waves incident on it from inside the problem domain, facilitates simulation of the infinite extent of the problem domain in the positive and the negative \mathbf{e}_3 directions. The TRBC consists of multiple bilayers of thickness a (see Fig. 1b). Thicknesses of the high and the low porosity layers within a bilayer are a_1 and a_2 , respectively. Two different microstructures of a bilayer are considered in the current study. For the sake of brevity, only one microstructure is shown in Fig. 1b. The next section describes the two microstructures in detail. The lengths of the domain in the \mathbf{e}_1 and the \mathbf{e}_2 directions, i.e., w_1 and w_2 , respectively, are chosen such that one unit of the

periodic microstructure along the in-plane directions is inside the problem domain (Fig. 1b).

The transient evolution of electromagnetic fields inside the problem domain is governed by Maxwell’s equations 1–4 (Jackson 1998).

$$\nabla \cdot \mathbf{B}(\mathbf{x}, t) = 0, \tag{1}$$

$$\nabla \times \mathbf{E}(\mathbf{x}, t) + \partial \mathbf{B}(\mathbf{x}, t) / \partial t = \mathbf{0}, \tag{2}$$

$$\nabla \cdot \mathbf{D}(\mathbf{x}, t) = 0, \tag{3}$$

$$\nabla \times \mathbf{H}(\mathbf{x}, t) - \partial \mathbf{D}(\mathbf{x}, t) / \partial t = \mathbf{J}, \tag{4}$$

where \mathbf{E} is the electric field, \mathbf{H} is the magnetic field, \mathbf{J} is the current density, $\mathbf{x} = x_1 \mathbf{e}_1 + x_2 \mathbf{e}_2 + x_3 \mathbf{e}_3$ is the position vector of a point in the problem domain, and t is the time.

The electric displacement field \mathbf{D} and the magnetic induction field \mathbf{B} are related to \mathbf{E} and \mathbf{H} , respectively, through the following constitutive relations:

$$\mathbf{D} = \epsilon_0 \boldsymbol{\epsilon}(\mathbf{x}) \mathbf{E}, \tag{5}$$

$$\mathbf{B} = \mu_0 \boldsymbol{\mu}(\mathbf{x}) \mathbf{H}, \quad (6)$$

where $\boldsymbol{\varepsilon}(\mathbf{x})$ is the relative dielectric constant tensor, ε_0 is the absolute dielectric constant, $\boldsymbol{\mu}(\mathbf{x})$ is the relative magnetic permeability tensor, and μ_0 is the absolute magnetic permeability. The current study only considers nonmagnetic materials for which $\boldsymbol{\mu}(\mathbf{x}) = \mathbf{I}$, where \mathbf{I} is the identity matrix. The current density \mathbf{J} is related to \mathbf{E} through the following constitutive relation:

$$\mathbf{J} = \boldsymbol{\sigma}(\mathbf{x}) \mathbf{E}, \quad (7)$$

where $\boldsymbol{\sigma}$ is the effective conductivity tensor of the medium. One notes that the effective conductivity $\boldsymbol{\sigma}$ combines the effects of electrical conductivity and loss due to absorption of electromagnetic waves in a lossy medium (Inan and Inan 2000; Modest 2003). In the current study, the material of the PBG crystal, i.e., Al_2O_3 is considered a lossless dielectric material, for which $\boldsymbol{\sigma} = 0$ (Harman et al. 1994; von Blanckenhagen et al., 2002). One also notes that for an isotropic material $\boldsymbol{\varepsilon}(\mathbf{x}) = \varepsilon(\mathbf{x}) \mathbf{I}$ and $\boldsymbol{\sigma}(\mathbf{x}) = \sigma(\mathbf{x}) \mathbf{I}$.

Periodic boundary conditions are applied on the vertical boundaries, i.e., $x_i = \pm w_i/2$, $i = 1$ and 2 , of the problem domain such that \mathbf{E} and \mathbf{H} on the boundary $x_i = +w_i/2$ are the same as those on the boundary $x_i = -w_i/2$. The periodic boundary conditions facilitate simulation of the infinite extent of the TRBC and the substrate along the \mathbf{e}_1 and the \mathbf{e}_2 directions. The boundary conditions on the domain at the positive and the negative extremities of the \mathbf{e}_3 direction are $\mathbf{H} \cdot \mathbf{n}_o = 0$ and $\mathbf{E} \times \mathbf{n}_o = \mathbf{0}$, where \mathbf{n}_o is the outward unit normal vector on the boundary.

Initially, the electric and the magnetic fields are zero inside the problem domain. To compute the reflectivity ρ , a Gaussian electromagnetic wave propagating along the \mathbf{e}_3 direction with a broad range of frequency is generated from a current source (Taflov and Hagness 2000) situated at a plane, which is marked as S in Fig. 1, parallel to the TRBC. Part of the wave propagating along the positive \mathbf{e}_3 -direction is reflected back from the TRBC and the rest propagates into the substrate and is absorbed in the PML at the extremity of the problem domain in the positive \mathbf{e}_3 direction. The reflectivity ρ is defined as the fraction of incident energy reflected (Robert Siegel 2002). The wave propagating along the negative \mathbf{e}_3 -direction is absorbed in the PML at the extremity of the problem domain in the negative \mathbf{e}_3 direction.

The 3-D domain considered above can be reduced to a 1-D domain along the \mathbf{e}_3 -direction by homogenizing each layer of the TRBC. In the current study, the Maxwell-Garnett (Garnett 1904) homogenization method is used to estimate the effective relative dielectric constant of each homogenized layer. One notes that the homogenized layers are transversely isotropic with the axis of transverse isotropy along the \mathbf{e}_3 -direction. Thus, the effective relative

dielectric constant is the same in the \mathbf{e}_1 and the \mathbf{e}_2 directions and is denoted by ε_p^e , which is given by Eq. 8 (Garnett 1904; Bruggeman 1935; Niklasson et al. 1981; Aspnes 1982; Dunn and Taya 1993).

$$\left(\varepsilon_p^e - \varepsilon_m \right) / \left(\varepsilon_p^e + \varepsilon_m \right) = V_p (\varepsilon_a - \varepsilon_m) / (\varepsilon_a + \varepsilon_m), \quad (8)$$

where $\varepsilon_a = 1.0$ is the relative dielectric constant of air, ε_m is the relative dielectric constant of the material of the PBG crystal, V_p is the porosity of layer p . Here $p = 1$ and 2 denote, respectively, the high and the low porosity layers within a bilayer. The expression for effective relative dielectric constant $\hat{\varepsilon}_p^e$ along the \mathbf{e}_3 -direction is given by Eq. 9.

$$\hat{\varepsilon}_p^e = V_p \varepsilon_a + (1 - V_p) \varepsilon_m \quad (9)$$

In the current study, electromagnetic wave propagation only along the \mathbf{e}_3 direction is considered, therefore, due to the transversality condition (Inan and Inan 2000) \mathbf{e}_3 components of the electric and the magnetic fields are zero for all the problems considered in subsequent sections. Thus, $\hat{\varepsilon}_p^e$ does not affect results reported in this article.

Computation of band gaps of a PBG crystal

A band gap is the range of frequency for which no wave vector exists for an electromagnetic wave inside the PBG crystal. The band gap is found by computing the variation of the frequency ω versus the wave vector \mathbf{k} . To this end, an eigenvalue problem in terms of only the magnetic field \mathbf{H} is derived from Eqs. 2 and 4 as briefly described here. Considering a time dependence $e^{-i\omega t}$ of the magnetic field, exploiting the periodicity of the microstructure and using Bloch's theorem, the magnetic field $\mathbf{H}(\mathbf{x})$ can be expressed as (Johnson and Joannopoulos 2001):

$$\mathbf{H}(\mathbf{x}, t) = \mathbf{u}(\mathbf{x}) e^{i(\mathbf{k} \cdot \mathbf{x} - \omega t)}, \quad (10)$$

where $\mathbf{u}(\mathbf{x})$ is a periodic function such that:

$$\mathbf{u}(\mathbf{x}) = \mathbf{u}(\mathbf{x} + \mathbf{R}). \quad (11)$$

In Eq. 11, $\mathbf{R} = \alpha \mathbf{r}_1 + \beta \mathbf{r}_2 + \gamma \mathbf{r}_3$ is the lattice vector of the periodic microstructure; α, β, γ are integers, \mathbf{r}_i are the primitive lattice vectors (Kittel 1966), and \mathbf{k} is the wave vector:

$$\mathbf{k} = k_1 \mathbf{b}_1 + k_2 \mathbf{b}_2 + k_3 \mathbf{b}_3. \quad (12)$$

In Eq. 12, \mathbf{b}_i is the primitive reciprocal lattice vectors and are related to \mathbf{r}_i through the following relationship (Kittel 1966):

$$\mathbf{r}_i \cdot \mathbf{b}_j = 2\pi \delta_{ij}. \quad (13)$$

Using Eqs. 10–12, Maxwell's equations 2 and 4 reduce to (Johnson and Joannopoulos 2001):

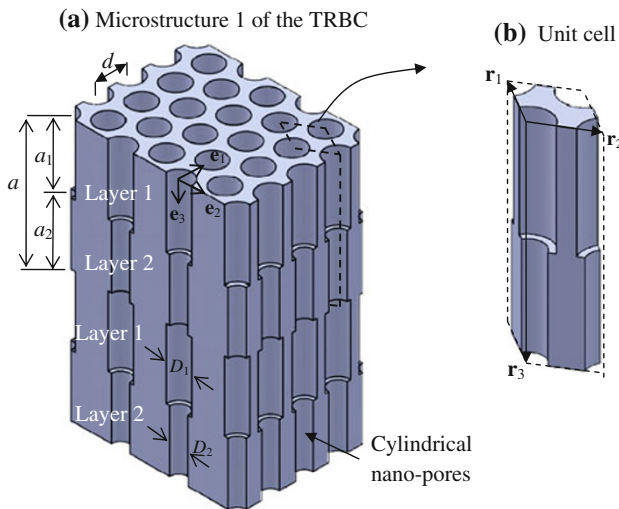


Fig. 2 **a** Microstructure 1 consisting of concentric cylindrical nano-pores, **b** the unit cell of microstructure 1

$$\hat{\Theta}_{\mathbf{k}} \mathbf{u}(\mathbf{x}) = \left(\frac{\omega(\mathbf{k})}{c} \right)^2 \mathbf{u}(\mathbf{x}), \tag{14}$$

where the differential operator $\hat{\Theta}_{\mathbf{k}}$, which depends on the wave vector \mathbf{k} , is given by:

$$\hat{\Theta}_{\mathbf{k}} = (i\mathbf{k} + \nabla) \times \left(\frac{1}{\epsilon_m} (i\mathbf{k} + \nabla) \times \right). \tag{15}$$

The eigenvalue problem (14) is solved on a unit cell of the periodic microstructure implicitly assuming that the microstructure is of infinite extent.

Two different periodic microstructures, which are shown in Figs. 2 and 3, respectively, are considered in the current study. Microstructure 1 (Fig. 2) is constructed such that the inter-pore distance d_1 in the high porosity layer (layer 1) and d_2 in the low porosity layer (layer 2) are the same, i.e. $d_1 = d_2 = d$. The diameter D_1 of pores in layer 1 is greater than D_2 in layer 2. The number of pores in a unit area parallel to the \mathbf{e}_1 – \mathbf{e}_2 plane is the same in both the layers. Microstructure 2 (Fig. 3) is constructed such that the inter-pore distance d_1 of layer 1 is smaller than the inter-pore distance d_2 of layer 2. In addition, the diameter D_1 of pores in layer 1 is smaller than D_2 in layer 2. Thus, the number of pores in a unit area parallel to the \mathbf{e}_1 – \mathbf{e}_2 plane is higher in layer 1 than that in layer 2. The smallest unit cells of the two microstructures considering only the translation operation are shown in Figs. 2b and 3b and are used as domains for the eigenvalue problem given by Eq. 14. The 3-D unit cells shown in Figs. 2b and 3b reduce to a 1-D unit cell (Fig. 4) when homogenized layers are

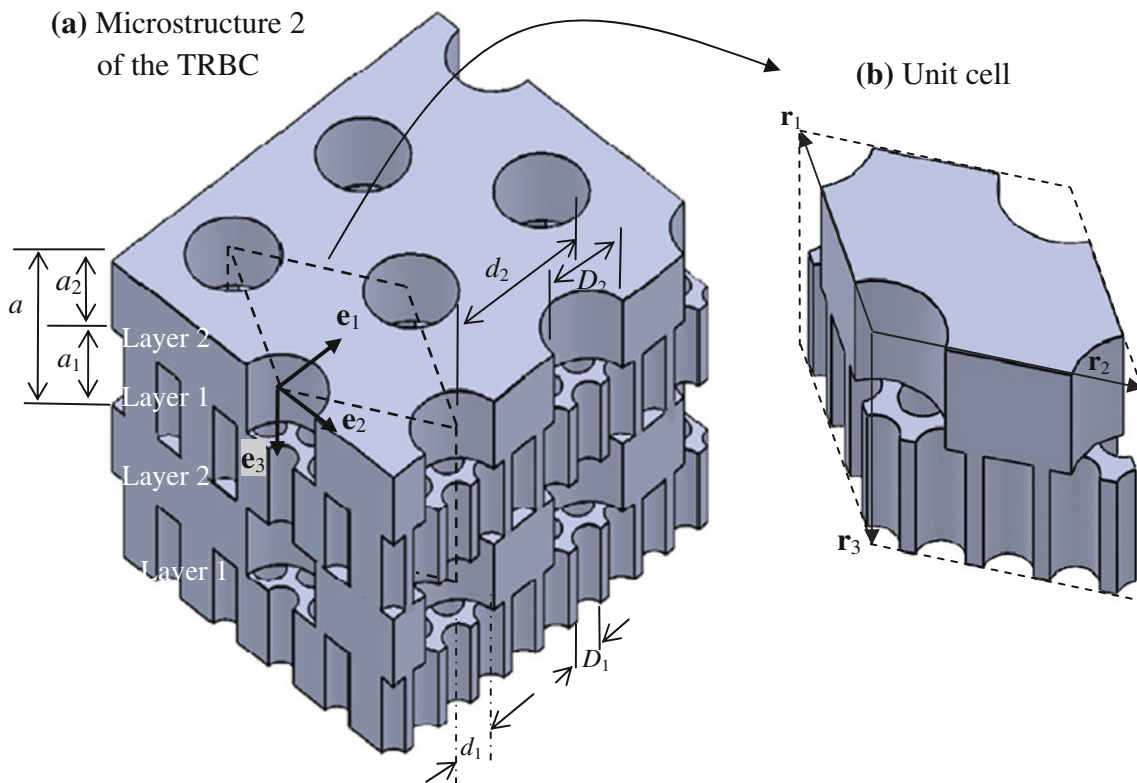


Fig. 3 **a** Microstructure 2 consisting of nano-porous layers of different inter-pore distances, **b** the unit cell of microstructure 2

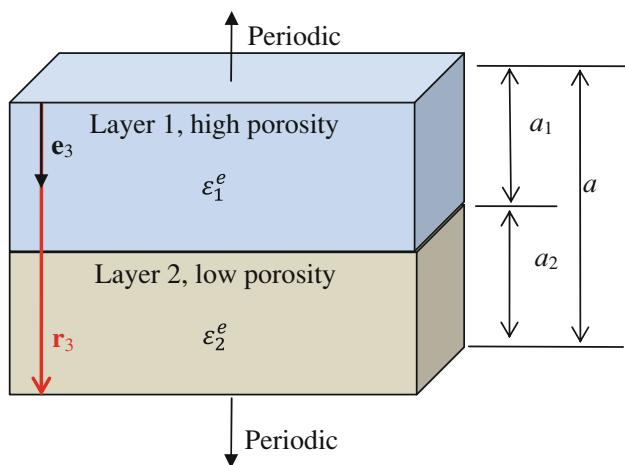


Fig. 4 The unit cell of the homogenized multi-layer microstructure

considered. The effective relative dielectric constant ε_p^e of the p th layer, where $p = 1$ or 2 , is estimated using Eq. 8 and the porosity $V_p = (\pi/2\sqrt{3})(D_p/d_p)^2$. The porosity V_p depends only on the ratio D_p/d_p .

The variation of the frequency $\omega_m(\mathbf{k})$, where m is the mode number, with \mathbf{k} can be obtained by solving the eigenvalue problem (14) for a range of values of \mathbf{k} . In the current study, the electromagnetic wave propagating along the \mathbf{e}_3 direction is considered and for subsequent analyses $\mathbf{k} = k_3\mathbf{b}_3$, where \mathbf{b}_3 is the reciprocal lattice vector along the \mathbf{e}_3 direction (Kittel 1966), is used. For brevity, we drop the subscript 3 from k_3 and k is used to denote a wave vector along \mathbf{b}_3 . One can show that $\omega_m(k)$ varies periodically with k such that $\omega_m(k) = \omega_m(k + n|\mathbf{b}_3|)$, $n = 1, 2, \dots$ and is symmetric about $k = |\mathbf{b}_3|/2$ (Joannopoulos et al. 1995). Therefore, variation of $\omega_m(k)$ for $0 \leq k \leq |\mathbf{b}_3|/2$ is presented in the subsequent sections.

Numerical solution of the governing equations

Equations 1–7 are solved to compute the reflectivity of the TRBC. For the 3-D microstructure considered in the current study, these equations cannot be solved analytically. Instead, the finite difference time domain (FDTD) method (Taflove and Hagness 2000) implemented in a freely available computer code known as MEEP (Oskooi et al. 2010) is used. To ensure that the error of the finite difference approximation is negligible, each simulation is carried out with successively refined finite difference grids such that the refined grid has twice the number of nodes in each direction than that of the previous grid until the maximum difference in reflectivities obtained from the two successive grids is $<3.0\%$. The time step is taken as half of the Courant time step (Taflove and Hagness 2000). In Fig. 1, the height h represents the separation between the source

plane S and the PML. In each simulation, h is kept at least as large as the largest wavelength considered in the simulation to ensure that the presence of the PML does not disturb the source at S. Similarly, the thickness h_p of the PML is kept at least as large as the largest wavelength to ensure that it is thick enough to absorb all incident waves (Oskooi et al. 2008). At least one simulation described in each subsequent section is repeated with h , h_s , and h_p (Fig. 1) equal to twice the largest wavelength to ensure that computed reflectivities are independent of h , h_s , and h_p .

The eigenvalue problem described by the partial differential equation 14 cannot be solved analytically except for a few simple microstructures. In the present work, Eq. 14 is solved with the plane-wave expansion method using a freely available computer code known as MPB (Johnson and Joannopoulos 2001). In the plane-wave expansion method, the partial differential equation is converted to a set of algebraic equations by expressing \mathbf{u} in terms of plane-wave basis. The computer code then computes the coefficient matrix using the discrete Fourier transform (DFT). Again, each simulation is carried out with successively refined grids used for DFT until the maximum difference in frequencies obtained from the two successive grids $<1.0\%$.

In the subsequent sections, unless stated otherwise, the coordinates of points of the problem domain are normalized by the bilayer thickness a of the microstructure (see Fig. 1) and results are reported using the normalized wave vector $ka/2\pi$ and the normalized frequency $\omega a/2\pi c$, where c is the speed of light in vacuum. The material property of Al_2O_3 is taken as $\varepsilon_m = 3.0$.

Analytical expression for the band gap of a homogenized multi-layer microstructure

Both the microstructures as shown in Figs. 2 and 3 can be considered as a stack of homogenized layers of alternating porosities of V_1 and V_2 with effective relative dielectric constants ε_1^e and ε_2^e , respectively (Fig. 4). Dielectric constants ε_1^e and ε_2^e are estimated using the Maxwell-Garnett method (Eq. 8). The ratio of the band gap width $\Delta\omega$ to the mid-gap frequency ω_{mid} of the homogenized layers for wave vectors parallel to the \mathbf{e}_3 direction is maximized if $a_1 n_1^e = a_2 n_2^e$ (Yeh 1988), where a_1 and a_2 are the layer thicknesses (Fig. 4) and $n_1^e (= \sqrt{\varepsilon_1^e})$ and $n_2^e (= \sqrt{\varepsilon_2^e})$ are refractive indices. The mid-gap frequency ω_{mid} and the maximum value of the ratio $\Delta\omega/\omega_{\text{mid}}$ are given by:

$$\omega_{\text{mid}} = \frac{n_1 + n_2}{4n_1 n_2} \cdot \frac{2\pi c}{a} \quad (16)$$

$$\Delta\omega/\omega_{\text{mid}} = \frac{4}{\pi} \sin^{-1} \left(\frac{|n_1 - n_2|}{n_1 + n_2} \right). \quad (17)$$

Results and discussions

In this section, reflectivities and band gaps are computed following the procedures described in “[Mathematical model](#)”. To gain insights into the effect of the pore size on the reflectivity, the reflectivity of a single semi-infinite layer of nano-porous material with a uniform porosity is studied in “[Reflectivity of a semi-infinite nano-porous layer](#)”. The band gaps of a PBG crystal of multi-layer microstructures are computed in “[Band gaps of a nano-porous periodic microstructure](#)”. In addition, reflectivities of multi-layer TRBCs are computed in “[Reflectivity of a multi-layer TRBC](#)”. Reflectivities of TRBCs and band gaps of PBG crystals for two different microstructures are computed by explicitly modeling the microstructures and are compared with those found considering homogenized layers to study the effect of microstructure on the reflectivity and the band gap.

Reflectivity of a semi-infinite nano-porous layer

To find the reflectivity of a semi-infinite nano-porous layer, the problem domain shown in Fig. 1 is modified. A nano-porous layer with constant diameter cylindrical pores with axes of pores parallel to the thickness direction replaces the TRBC and the substrate shown in Fig. 1. The modified domain is shown in Fig. 5a. The PML at the extremity of the problem domain in the positive \mathbf{e}_3 direction absorbs all

electromagnetic waves propagating through the nano-porous layer and mimic the infinite extent of nano-porous layer in the \mathbf{e}_3 direction (Oskooi et al. 2008). The thickness h_l of the layer (Fig. 5a) is kept at least as large as the largest wavelength considered in a simulation. Simulations are repeated with successively larger h_l to ensure that computed reflectivities are independent of h_l .

A nano-porous layer with porosity V can be replaced with a layer of homogenized material of effective relative dielectric constant ε^e estimated from the Maxwell-Garnett method (Eq. 8). As a single layer is considered, the subscript p from various terms of Eq. 8 is omitted. The analytical expression that is given by Modest (2003) for the reflectivity of a semi-infinite layer is used to compute the reflectivity of the homogenized layer.

Figure 6a shows variations of reflectivities of semi-infinite nano-porous layers of different porosities with the ratio λ/d , where λ is the wavelength $\lambda = 2\pi c/\omega$. It is evident from Fig. 6a that the reflectivity of the 65% porous layer estimated considering the microstructure explicitly is ~ 0.02 at $\lambda/d = \sim 0.6$ and increases as λ/d increases to ~ 0.8 . The reflectivity suddenly decreases at $\lambda/d = \sim 0.8$ and almost vanishes when the wavelength of incident wave is approximately the same as the inter-pore distance d (i.e., $\lambda/d = \sim 1.0$) due to the interaction of the microstructure with the incident wave. As the wavelength increases from $\lambda/d = \sim 1.0$, the reflectivity suddenly increases to ~ 0.015 at approximately $\lambda/d = \sim 1.2$. As the wavelength farther

Fig. 5 a A schematic of the problem domain used to compute the reflectivity of a semi-infinite layer, **b** the cross-sectional view of the nano-porous layer along a plane parallel to the \mathbf{e}_1 – \mathbf{e}_2 plane

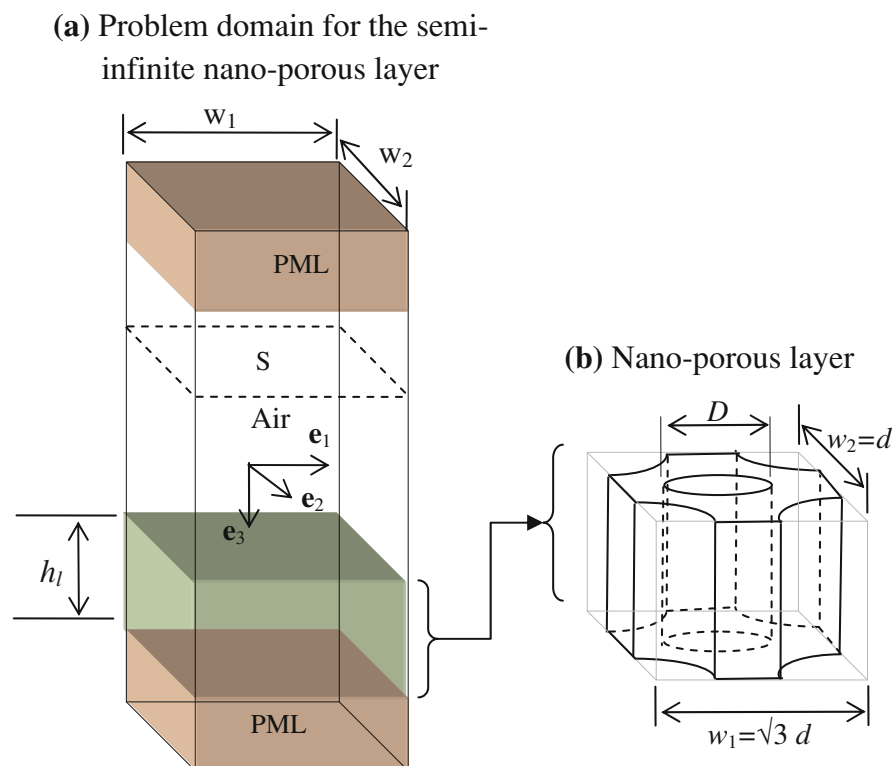
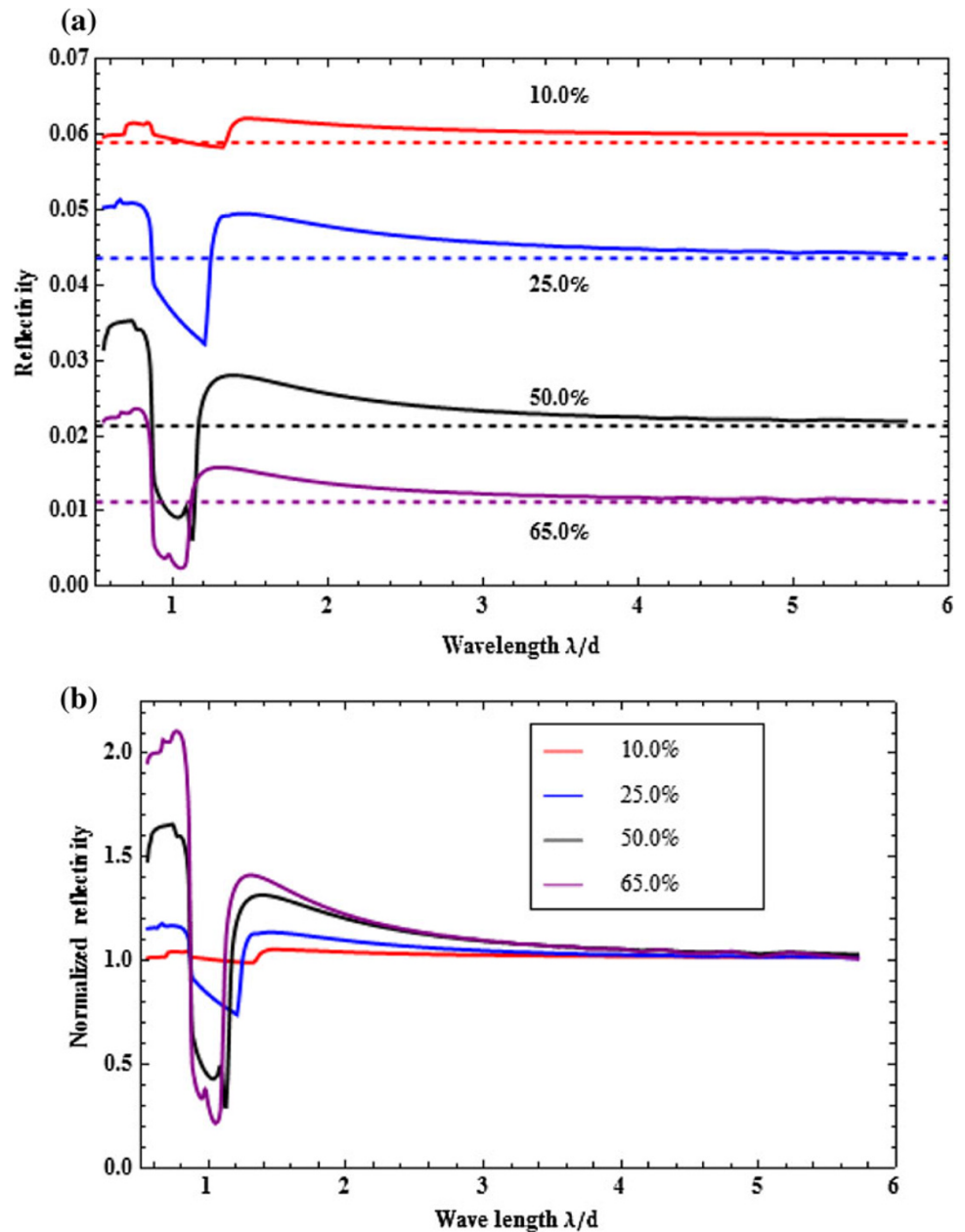


Fig. 6 Variations of **a** the reflectivity and **b** the normalized reflectivity of a semi-infinite nano-porous layer with the wavelength for porosities 10, 25, 50, and 65%; *solid lines* microstructure modeled explicitly; *dashed lines* homogenized layers



increases, the reflectivity gradually decreases. At the large wavelength limit (i.e., $\lambda/d > \sim 3.0$) the reflectivity of 65% porous layer estimated considering the microstructure explicitly compares well with that computed considering the homogenized layer. This behavior at the large wavelength is expected because the effective relative dielectric constant estimated from the Maxwell-Garnett homogenization method is expected to be accurate at the large wavelength limit. Reflectivities of porous layers with different porosities (i.e., 50, 25, and 10%) qualitatively follow the same trend as that of the 65% porous layer. To study the trend of the variation of the reflectivity for different porosities, reflectivities of nano-porous layers normalized

by reflectivities at the large wavelength limit are shown in Fig. 6b. It is evident from Fig. 6b that the sudden decrease of normalized reflectivities around $\lambda/d = \sim 1.0$ increases for increasing porosity. In addition, normalized reflectivities for the very short wavelength range (i.e., $\lambda/d < \sim 0.8$) increases with increasing porosity. For 65% porosity at $\lambda/d = \sim 0.8$, the reflectivity is approximately twice greater than that of the large wavelength limit. Similarly, normalized reflectivities in the intermediate wavelength range (i.e., $\sim 1.2 < \lambda/d < \sim 3.0$) are greater for higher porosities.

As the reflectivity is proportional to the dielectric constant of the layer, one can conclude that porous layers have

a higher dielectric constant than that estimated by the Maxwell-Garnett method for the very short wavelength range (i.e., $\lambda/d < \sim 0.8$) and for the intermediate wavelength range (i.e., $\sim 1.2 < \lambda/d < \sim 3.0$). On the other hand, for wavelengths approximately equal to the inter-pore distance (i.e., $\lambda/d = \sim 1.0$), porous layers have a significantly lower dielectric constant. For TRBC applications, the wavelength of incident thermal radiation is at least ~ 500 nm and the inter-pore distance d for nano-porous Al_2O_3 is at most ~ 250 nm; thus, the wavelength range of interest for such applications is $\lambda/d > \sim 2$. Therefore, the short wavelength range $\lambda/d < \sim 2$ is not of interest to the current study. The variation of the reflectivity of a porous layer with the wavelength in the range $\lambda/d > \sim 2$ can be exploited to generate a wider band gap from a multi-layer TRBC with alternate high and low porosity layers as explained below.

A multi-layer TRBC will have a wider band gap when the ratio of dielectric constants of the two adjacent layers is high (Joannopoulos et al. 1995). From the study of the reflectivity of a single porous layer, one can conclude that a higher contrast of dielectric constants between the two adjacent layers can be achieved by carefully selecting inter-pore distances of the high and the low porosity layers. The inter-pore distances can be selected in such a way that the dielectric constant of the high porosity layer is the minimum and that of the low porosity layer is the maximum for the incident wavelength. For example, if a multi-layer TRBC has alternate layers of 50 and 25% porosities and the wavelength λ of the incident wave is $0.5 \mu\text{m}$, then the inter-pore distance of the 50% porosity layer should be at least thrice smaller ($\lambda/d_1 > \sim 3.0$) than the wavelength of incident wave that is $d_1 < \sim 0.17 \mu\text{m}$ to minimize the

dielectric constant of the layer (see Fig. 6). On the other hand, the inter-pore distances of the 25% porosity layer should belong to the intermediate wavelength range (i.e., $\sim 1.2 < \lambda/d < \sim 3.0$) with respect to the incident wavelength that is $\sim 0.17 \mu\text{m} < d_2 < \sim 0.42 \mu\text{m}$ to maximize the dielectric constant of the layer (see Fig. 6).

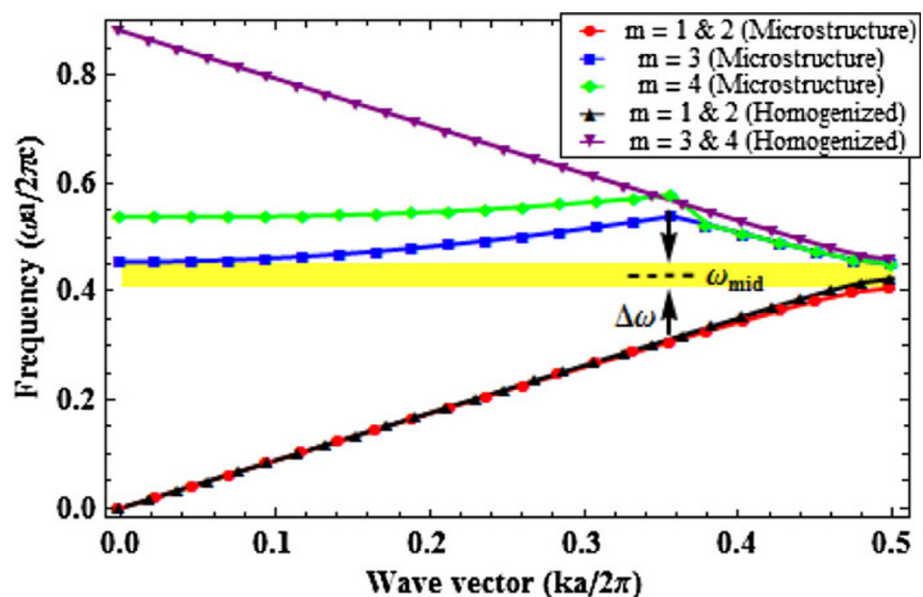
This strategy of widening of the band gap as described above requires the inter-pore distances of the low and the high porosity layers to be different. However, a multi-layer TRBC of concentric pores with the same inter-pore distance in both the low and the high porosity layers is easy to fabricate (Lee et al. 2006). In the next subsection, two different microstructures with different arrangements of pores are considered to explore the possibility of widening the band gap of a multi-layer film. The first microstructure (Fig. 2) has concentric pores with the same inter-pore distance d in both the low and the high porosity layers. Whereas, the second microstructure (Fig. 3) allows for different inter-pore distances in the high and the low porosity layers and implements the strategy of widening the band gap as explained in the last paragraph. In subsequent sections, detailed parametric studies by varying the ratio λ/d are reported to examine the effect of the inter-pore distances on the band gap.

Band gaps of a nano-porous periodic microstructure

The band gap of microstructure 1

Variations of frequencies $\omega_m(k)$ versus k are exhibited in Fig. 7 for microstructure 1 with inter-pore distance $d = 1.8a$ and porosities of layers alternating between $V_1 = 90\%$ and $V_2 = 68\%$. Here d , V_1 and V_2 are taken as

Fig. 7 Variations of the frequency with the wave vector for microstructure 1. The yellow band indicates the band gap when microstructure 1 is explicitly modeled



an example and in the next subsection, a detailed parametric study with various inter-pore distances and porosities is presented. Frequencies computed using the homogenized layers are also shown in Fig. 7. It is evident from Fig. 7, that no wave vector exists for the range of frequency $0.406 \leq \omega a/2\pi \leq 0.451$ when microstructure is considered explicitly; thus, this is a band gap for the microstructure. When the homogenized layers are considered, the band gap is $0.423 \leq \omega a/2\pi \leq 0.458$. Thus, the ratio of band gap width to the mid-gap frequency $\Delta\omega/\omega_{\text{mid}} = 10.50\%$ computed considering the microstructure explicitly is $\sim 27\%$ larger than $\Delta\omega/\omega_{\text{mid}} = 8.30\%$ computed from the homogenized layers. The band gaps computed considering the microstructure explicitly and the homogenized layers occur at $ka/2\pi = 0.5$.

One notes that the mid-gap frequency $\omega_{\text{mid}}a/2\pi c = 0.43$ exhibited in Fig. 7 corresponds to $\lambda_{\text{mid}}/d = 1.3$, which is in the intermediate wavelength range according to the discussions of “[Reflectivity of a semi-infinite nanoporous layer](#)”. It was shown in “[Reflectivity of a semi-infinite nano-porous layer](#)” that refractive indices of single porous layers in the intermediate wavelength range were greater when microstructures of layers were considered explicitly than those of the homogenized layers. Thus, the band gap of microstructure 1 computed considering the microstructure explicitly is greater than that found from the homogenized layers.

Since the effective relative dielectric constant of a homogenized layer is the same in the \mathbf{e}_1 - and the \mathbf{e}_2 -directions, there are degenerate frequencies because electromagnetic waves with polarization vectors along the \mathbf{e}_1 and the \mathbf{e}_2 directions are indistinguishable from each other with respect to the homogenized layers (Taflov and Hagness, 2000). Thus, frequencies for modes $m = 1$ and 2 and similarly $m = 3$ and 4 are the same. Numerical simulations reveal that frequencies for modes $m = 1$ and 2 are virtually indistinguishable when the microstructure is considered explicitly. In addition, for $m = 1$ and 2, frequencies computed considering the microstructure explicitly are in excellent agreement with those computed considering the homogenized layers. For $m = 3$ and 4, frequencies computed considering the microstructure explicitly are not in good agreement with those computed considering the homogenized layers for $0 \leq ka/2\pi < \sim 0.35$; however, this disagreement does not have a significant effect on the band gap at $ka/2\pi = 0.5$.

Effects of the pore size on the band gap of microstructure 1

Next, a parametric study of effects of the inter-pore distance d and different porosities on the band gap of microstructure 1 (Fig. 2) is reported. Five cases of different porosities (see Table 1) are considered. Porosities of

Table 1 Porosities and effective properties of layers

Layer p	Porosity V_p (%)
Case 1	
1	90
2	68
Case 2	
1	75
2	52
Case 3	
1	65
2	41
Case 4	
1	50
2	25
Case 5	
1	35
2	9

different cases are chosen such that the ratio of refractive indices of the two adjacent layers is 1.14 for all five cases; thus, according to Eq. 17, $\Delta\omega/\omega_{\text{mid}} = 8.30\%$ for all cases when homogenized layers are considered.

Figures 8 and 9 show variations of mid-gap wavelengths and band gaps with d for the five cases. From the Fig. 8, it is clear that for all the five cases mid-gap wavelengths λ_{mid} are more than thrice larger than the inter-pore distance d (i.e., $\lambda_{\text{mid}}/d > \sim 3.0$) when d/a is less than approximately 0.8. Therefore, for $d/a < 0.8$, the band gap wavelengths are in the large wavelength range as discussed in “[Reflectivity of a semi-infinite nano-porous layer](#)”. Thus, the effective relative dielectric constants of homogenized layers are expected to be accurate and band gaps computed using the homogenized layers compare well with that found from the explicit consideration of the microstructure for $d/a < 0.8$ as shown in Fig. 9.

For $\sim 0.8 < d/a < \sim 1.8$, the mid-gap wavelengths are in between ~ 3.0 and ~ 1.2 (Fig. 8) times larger than the inter-pore distance d ; thus they fall in the intermediate wavelength range according to the discussion of “[Reflectivity of a semi-infinite nano-porous layer](#)”. Therefore, effective relative dielectric constants of the homogenized layers are not expected to be accurate and band gaps computed from explicit considerations of the microstructure deviate from that computed considering the homogenized layers for $\sim 0.8 < d/a < \sim 1.8$ as shown in Fig. 9. For cases 1, 2 and 3, band gaps computed considering the microstructure explicitly decrease with increasing d/a . On the other hand, for cases 4 and 5, the band gaps computed considering the microstructure explicitly increase with increasing d/a up to $d/a = \sim 1.8$. For case 5, with $V_1 = 90\%$, $V_2 = 68\%$, the maximum

Fig. 8 Variations of the ratio of mid-gap wavelengths to the inter-pore distance d of microstructure 1 with the normalized inter-pore distance d/a

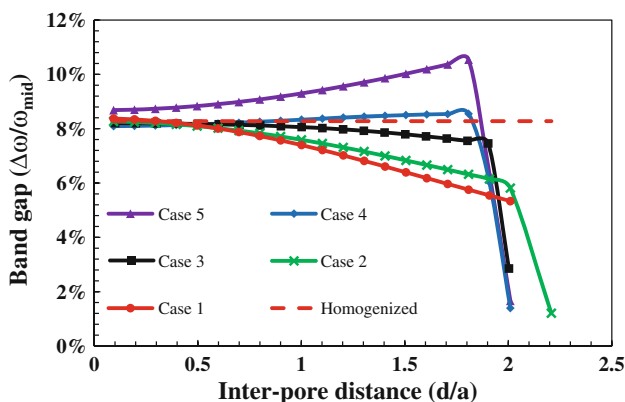
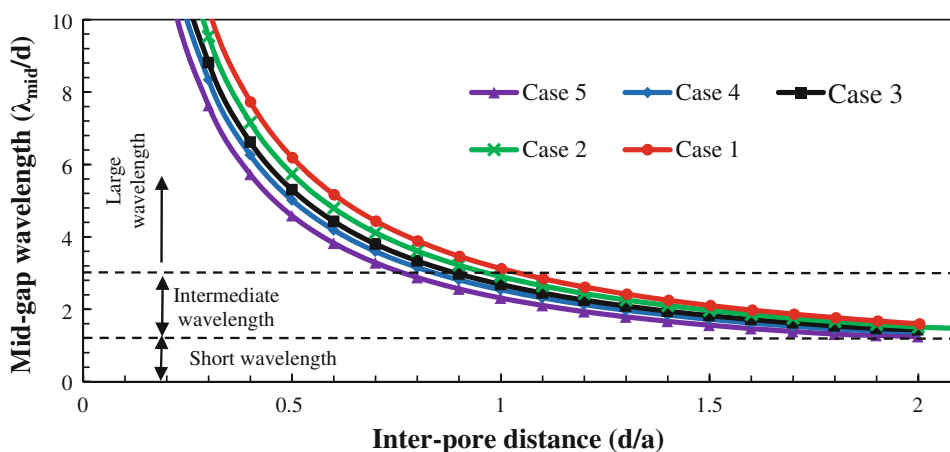


Fig. 9 Variations of the band gap of microstructure 1 with the normalized inter-pore distance d/a for various porosities

$\Delta\omega/\omega_{mid} = \sim 10.50\%$ is $\sim 27\%$ larger than that found from the homogenized layers. Thus, a larger porosity (i.e., $V_1 = 90\%$, $V_2 = 68\%$) and $d/a = \sim 1.8$ generate a larger band gap than other values of porosities and d/a ratios considered.

For $d/a > 1.8$, it is clear from Fig. 8 that $\sim 1 < \lambda_{mid}/d < \sim 1.2$; thus the band gap wavelengths belong to the short wavelength range according to the discussions of “Reflectivity of a semi-infinite nano-porous layer”. In “Reflectivity of a semi-infinite nano-porous layer”, it was shown that the refractive index of a single layer of the microstructure was significantly smaller in the short wavelength range than that in the large wavelength range. Similarly, it is observed from Fig. 9 that the band gaps for $d/a > \sim 1.8$ rapidly decrease with increasing d/a .

For all the five cases considered above, layer thicknesses a_1 and a_2 were chosen such that $a_1/a_2 = n_2^e/n_1^e$. A parametric study considering case 5 was conducted by varying a_1/a_2 from 0.1 to 0.9 and keeping $d/a = 1.8$. This study showed that the band gap reported in Fig. 9 at $d/a = 1.8$ for case 5 could not be significantly increased by varying a_1/a_2 . Therefore, the band gap reported for case 5 at

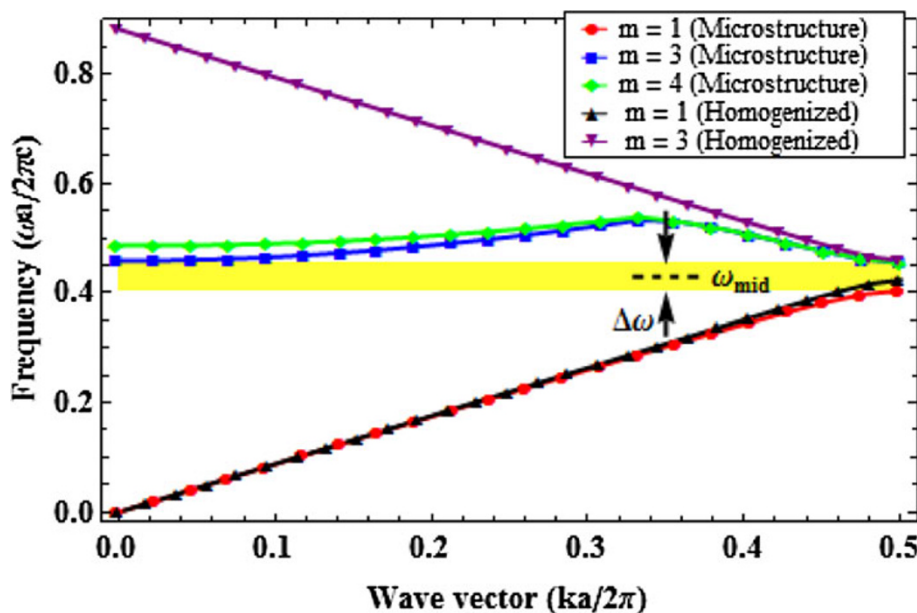
$d/a = 1.8$ (see Fig. 9) is the maximum for all values of a_1/a_2 . For the sake of brevity, details of this parametric study are not reported here.

The band gap of microstructure 2

Variations of frequencies $\omega_m(k)$ versus k are exhibited in Fig. 10 for microstructure 2 with inter-pore distance $d_1 = 0.5a$, $d_2 = 2a$ and the porosities of the two adjacent layers $V_1 = 90\%$ and $V_2 = 68\%$. Here d_1, d_2, V_1 and V_2 are taken as an example and in the next subsection, a detailed parametric study with various inter-pore distances and porosities is presented. Frequencies computed using the homogenized layers are also shown in Fig. 10. It is evident from Fig. 10 that no wave vector exists for the range of the frequency $0.403 \leq \omega a/2\pi \leq 0.455$ when microstructure is considered explicitly; thus, this is a band gap for the microstructure. The ratio of band gap width to the mid-gap frequency $\Delta\omega/\omega_{mid} = 12.04\%$ computed considering the microstructure explicitly is $\sim 50\%$ larger than $\Delta\omega/\omega_{mid} = 8.08\%$ computed from the homogenized layers. The band gap computed considering the microstructure explicitly and the homogenized layers occur at $ka/2\pi = 0.5$.

One notes that the mid-gap frequency $\omega_{mid}a/2\pi c = 0.43$ exhibited in Fig. 10 corresponds to $\lambda_{mid}/d_1 = \sim 4.6$ and $\lambda_{mid}/d_2 = \sim 1.2$. This means λ_{mid} belongs to the large wavelength range with respect to the inter-pore distance d_1 and to the intermediate wavelength range with respect to the inter-pore distance d_2 as discussed in “Reflectivity of a semi-infinite nano-porous layer”. According the discussion of “Reflectivity of a semi-infinite nano-porous layer”, these selections of inter-pore distances d_1 and d_2 increase the ratio of refractive indices of the two adjacent layers. Therefore, band gaps computed considering the microstructure explicitly are greater than those computed considering homogenized layers. In comparison, microstructure 1 was constructed such that the mid-gap wavelength was in the intermediate wavelength range with

Fig. 10 Variations of the frequency with the wave vector for microstructure 2. The yellow band indicates the band gap



respect to the inter-pore distance d , which was same in both layers. The microstructure 2 with $d_1 = 0.5a$, $d_2 = 1.8a$, $V_1 = 90\%$ and $V_2 = 68\%$ has the advantage of having a 15% larger band gap than that of the microstructure 1 with $d = 1.8a$, and the same porosities.

Similar to the results found for microstructure 1, numerical simulations reveal that frequencies for modes $m = 1$ and 2 are virtually indistinguishable when microstructure 2 is considered explicitly. In addition, for $m = 1$ and 2, frequencies computed considering the microstructure explicitly are in good agreement with those computed considering the homogenized layers. For $m = 3$ and 4, frequencies computed considering the microstructure explicitly are not in good agreement with those computed considering the homogenized layers; however, similar to the result of microstructure 1, this disagreement does not have a significant effect on the band gap at $ka/2\pi = 0.5$.

Effects of the pore size on the band gap of microstructure 2

Next, a parametric study of the effect of the inter-pore distance d_1 and d_2 on the band gap of microstructure 2 is reported. Porosities of the multi-layer microstructure of the five cases considered in this subsection are the same as those considered in “Effects of the pore size on the band gap of microstructure 1” (Table 1). In the parametric study, the ratio d_2/a is varied from 0.2 to 2.25 and the ratio d_1/d_2 is kept constant at 0.25. Figures 11 and 12 show variations of mid-gap wavelengths normalized by d_1 and d_2 , respectively, with the inter-pore distance d_2 for various porosities. Figure 13 shows variations of band gaps for the five cases with d_2 . From Fig. 11, it is clear that mid-gap wavelengths λ_{mid} are more than thrice larger than the inter-

pore distances d_1 for all values of d_2/a considered; thus, the mid-gap wavelength is always in the large wavelength range with respect to the inter-pore distance d_1 of layer 1. Therefore, the effective dielectric constant of the layer 1 is expected to be accurate. On the other hand, it is evident from Fig. 12 that mid-gap wavelengths λ_{mid} are not always in the large wavelength range with respect to d_2 ; thus, the effective dielectric constant of the layer 2 is not always expected to be accurate.

From Fig. 12, it is clear that when d_2/a is less than approximately 0.8, the mid-gap wavelengths are in the large wavelength range with respect to the inter-pore distance d_2 . Thus, for $d_2/a < 0.8$, effective relative dielectric constants of both the layers are expected to be accurate, and band gaps computed from explicit considerations of the microstructure compare well with that found using the homogenized layers for $d_2/a < 0.8$ as shown in Fig. 13.

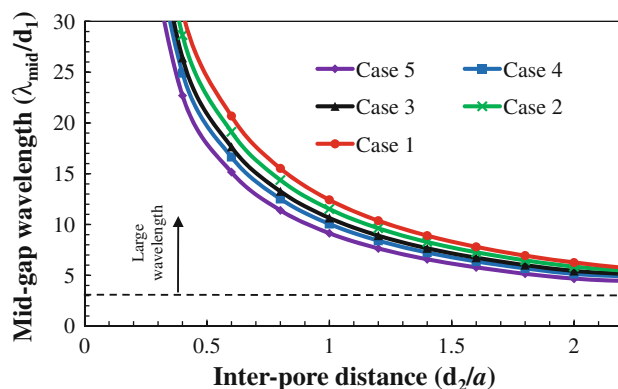


Fig. 11 Variations of the ratio of mid-gap wavelengths to the inter-pore distance d_1 of microstructure 2 with the normalized inter-pore distance d_2/a

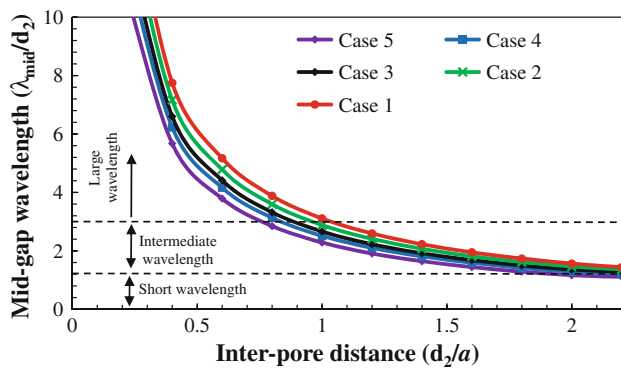


Fig. 12 Variations of the ratio of mid-gap wavelengths to the inter-pore distance d_2 of microstructure 2 with the normalized inter-pore distance d_2/a

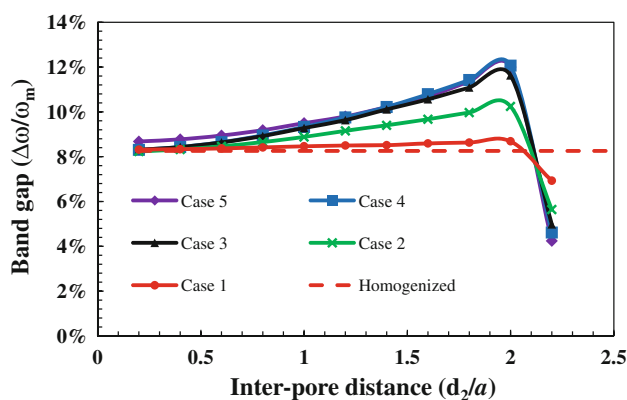


Fig. 13 Variations of the band gap of the microstructure 2 with the normalized inter-pore distance d_2/a

For $\sim 0.8 < d_2/a < \sim 2.0$, the mid-gap wavelengths are between ~ 3.0 and ~ 1.2 (Fig. 12) times larger than d_2 ; thus they fall in the intermediate wavelength range according to the discussion of “[Reflectivity of a semi-infinite nano-porous layer](#)”. Therefore, according to the discussion of “[Reflectivity of a semi-infinite nano-porous layer](#)”, the effective dielectric constant of layer 2 is not expected to be accurate and it is clear from Fig. 13 that for $\sim 0.8 < d/a < \sim 2.0$, band gaps computed from explicit considerations of the microstructure deviate from that computed considering the homogenized layers. For the all five cases, the band gaps computed considering the microstructure explicitly increase with increasing d_2/a up to $d_2/a = 2.0$. For case 5, the maximum $\Delta\omega/\omega_{\text{mid}} = \sim 12.0\%$ (at $d_2/a = 2.0$) is approximately 45% larger than that found from the homogenized layers. Thus, a larger porosity (i.e., $V_1 = 90\%$, $V_2 = 68\%$) and $d_2/a = 2.0$ generate a significantly larger band gap than other values of porosities and d_2/a ratios considered in this subsection.

For $d_2/a > 2.0$, it is clear from Fig. 12 that $\lambda_{\text{mid}}/d_2 < \sim 1.2$; thus, band gap wavelengths belong to the short

wavelength range according to the discussions of “[Reflectivity of a semi-infinite nano-porous layer](#)”. In “[Reflectivity of a semi-infinite nano-porous layer](#)”, it was shown that range of the refractive index of a single layer of the microstructure was considerably smaller than that of the homogenized layer in the short wavelength. Similarly, it is observed from Fig. 13 that the band gaps for $d/a > 2.0$ rapidly decrease with an increase in d_2/a .

For all the five cases considered above, layer thicknesses a_1 and a_2 were chosen such that $a_1/a_2 = n_2^e/n_1^e$. A parametric study was conducted by varying a_1/a_2 from 0.1 to 0.9 and keeping $d_2/a = 2.0$ and $d_1/d_2 = 0.25$. The study showed that the maximum band gaps reported in Fig. 13 at $d_2/a = 2.0$ were not significantly increased by varying the ratio a_1/a_2 . In addition, band gaps were also computed for $d_1/d_2 = 0.17$, but no significant difference in results was found from those reported in Fig. 13. Therefore, the band gap reported in Fig. 13 at $d_2/a = 2.0$ for each of the five cases can be considered the maximum band gap for the microstructure for each case. For the sake of brevity, details of these parametric studies with different values of a_1/a_2 and d_1/d_2 are not reported here.

In summary, microstructure 2 has a wider band gap than that of microstructure 1 for all the different porosities considered. Among all the different porosities, configurations of pores and inter-pore distances studied, the microstructure 2 has the maximum band gap when $d_2/a = 2.0$, $V_1 = 90\%$, and $V_2 = 68\%$. The maximum band gap computed considering the microstructure explicitly is $\sim 45\%$ larger than that found considering the homogenized layers.

Reflectivity of a multi-layer TRBC

Band gaps as presented in the previous section are estimated assuming that the microstructures are of infinite extent. In reality, only a finite number of layers can be used as a reflective film. Cornelius and Dowling (1999) studied modification of reflectivity of a substrate ($\epsilon = 9.0$ and $\sigma = 0.2$) with a multi-layer film with ratio of refractive indices of two adjacent layers of 1.5. They demonstrated that increasing the number of bilayers from one to five increased the maximum reflectivity from ~ 0.3 to ~ 0.7 . In comparison, the substrate without the multi-layer film had a reflectivity of 0.25. In this section, the reflectivity of a TRBC of ten bilayers (referring to Fig. 1, $n = 10$) situated over a substrate with material properties $\epsilon = 9.0$ and $\sigma = 0.2$ is studied. Two microstructures as shown in Figs. 2 and 3 with porosities and inter-pore distances as reported in “[The band gap of microstructure 1](#)” and “[The band gap of microstructure 2](#)”, respectively, are considered.

Reflectivities of TRBCs of the two different microstructures (Figs. 3 and 4) are computed following the procedure described in “[Computation of reflectivity of a multi-layer TRBC](#)”

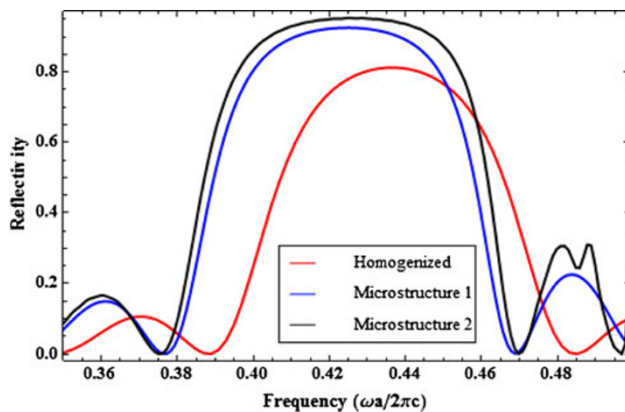


Fig. 14 The variations of the reflectivity with the wavelength of incident radiation for the TRBC with ten bilayers

and are plotted against frequency in Fig. 14. The reflectivity computed considering the TRBC as a stack of homogenized layers with effective relative dielectric constants estimated from the Maxwell-Garnett method is also plotted in Fig. 14. It is evident from Fig. 14 that increased reflectivities are observed centered on the mid-gap frequencies of ~ 4.2 for the microstructures and ~ 4.4 for the homogenized layers. Maximum reflectivity of ~ 0.95 for microstructure 2 is very close to ~ 0.92 of microstructure 1 and is $\sim 16\%$ higher than ~ 0.80 found from the homogenized layers. It is clear from Fig. 14 that the increased reflectivity is observed over a wider range of frequencies for both the microstructures than that observed for the homogenized layers. Therefore, similar to the studies of “Band gaps of a nano-porous periodic microstructure”, where it is found that the explicit consideration of microstructures 1 and 2 with $V_1 = 90\%$ $V_2 = 68\%$ have larger band gap width than that for the homogenized layers; a TRBC also has higher reflectivity over a wider range of frequencies when the microstructures are considered explicitly than that when homogenized layers are considered. It is worthwhile to note here that in Fig. 14, the non-dimensional frequency is used to report variations of reflectivities. For a particular high temperature application, one can choose the bi-layer thickness a of the microstructure such that higher reflectivity is in the wavelength range of the incident thermal radiation to effectively reflect the incident energy. For example, a TRBC with $a = 1 \mu\text{m}$ with either microstructure 1 or 2 will have a higher reflectivity for the wavelength range of 2.15 to 2.65 μm .

Conclusions

A highly reflective TRBC placed over a typical thermal barrier coating can significantly reduce heat transfer to the structure from the high temperature environment. This

paper explored the possibility of tailoring the reflectivity of a TRBC of a PBG crystal, which is a three dimensional periodic microstructure of cylindrical pores. The microstructure is such that the TRBC can be considered as a stack of multiple layers with low and high porosities. The primary motivation behind considering this microstructure was that it could be fabricated using aluminum dioxide, which remains stable at high temperatures (e.g., $>1,500 \text{ K}$). The governing equations of the electromagnetic theory for computation of the band gap and the reflectivity were summarized. Both closed form solutions and computer simulations were used to determine the effects of microstructure on the band gap of the PBG crystal and the reflectivity of the TRBC.

To gain an insight into the effect of the microstructure of a nano-porous layer on its reflectivity, the reflectivity of a semi-infinite layer with uniform porosity was computed by explicitly modeling the microstructure and was compared with that computed considering a homogenized layer. The effective dielectric constant of the homogenized layer was estimated using the Maxwell-Garnett homogenization method. When the wavelength of the incident radiation was significantly greater than (i.e., greater than three times) the inter-pore distance between the cylindrical pores, the reflectivity computed considering the microstructure explicitly agreed well with that of the homogenized layer. If the wavelength of incident radiation was between ~ 1.2 and ~ 3.0 times larger than the inter-pore distance, the reflectivity computed considering the microstructure explicitly was significantly greater than that computed using the homogenized layer.

The band gaps and the reflectivity of multi-layer TRBCs were computed for two different arrangements of nanopores by considering microstructures explicitly and homogenized layers. Microstructure 1 was constructed such that the diameter of pores in the high porosity layer was larger than that of the low porosity layer and there was same number of pores in a unit in-plane area of both the high and the low porosity layers. Microstructure 2 was constructed such that the diameter of pores in the high porosity layer was smaller than that of the low porosity layer and there was higher number of pores in a unit in-plane area of the high porosity layer than that of the low porosity layer. Parametric studies on various porosities and inter-pore distances revealed that the band gap width of microstructure 1 was about 25% higher than that of the homogenized layers when the porosities of layers alternated between ~ 70 and $\sim 90\%$. In this case, the inter-pore distance of both the low and the high porosity layers was approximately 1.3 times larger than the mid-gap wavelength. In addition, it was shown that the band gap width of microstructure 2 was about 45% higher than that of the homogenized layers when the porosities of layers

alternated between ~ 70 and $\sim 90\%$. In this case, the inter-pore distance in the low porosity layer was approximately twice larger than the mid-gap wavelength and that of the high porosity layer was significantly larger than the mid-gap wavelength. Similarly, the reflectivity a TRBC with microstructure 2 was significantly larger than that found from the homogenized layers.

Acknowledgments Authors thank Mr. Edwin Alexander Peraza Hernandez for preparing schematics of microstructures. This work was supported by the Multidisciplinary University Research Initiative grant FA9550-09-1-0686 from the Air Force Office of Scientific Research to the Texas A & M University with Dr. David Stargel as the program manager.

Open Access This article is distributed under the terms of the Creative Commons Attribution License which permits any use, distribution and reproduction in any medium, provided the original author(s) and source are credited.

References

- Aspnes DE (1982) Local-field effects and effective-medium theory: a microscopic perspective. *Am J Phys* 50(8):704–709
- Berenger J-P (1994) A perfectly matched layer for the absorption of electromagnetic waves. *J Comput Phys* 114(2):185–200
- Breggeman DAG (1935) Dielectric constant and conductivity of mixtures of isotropic materials. *Ann Phys (Leipzig)* 24:636–679
- Chen TM (1997) Radiative heat transfer in absorbing, emitting, and anisotropically scattering boundary-layer flows with reflecting boundary. *Heat Mass Transf* 32(6):411–417
- Cornelius CM, Dowling JP (1999) Modification of Planck blackbody radiation by photonic band-gap structures. *Phys Rev A* 59(6):4736
- Datta S, Chan CT, Ho KM, Soukoulis CM (1992) Photonic band gaps in periodic dielectric structures: The scalar-wave approximation. *Phys Rev B* 46(17):10650
- Dunn ML, Taya M (1993) Micromechanics predictions of the effective electroelastic moduli of piezoelectric composites. *Int J Solids Struct* 30(2):161–175
- Garnett JCM (1904) Colours in Metal Glasses and in Metallic Films. *Philosophical Transactions of the Royal Society of London Series A, Containing Papers of a Mathematical or Physical Character* 203(359–371):385–420
- Guo S, Albin S (2003) Simple plane wave implementation for photonic crystal calculations. *Opt Express* 11(2):167–175
- Harman AK, Ninomiya S, Adachi S (1994) Optical constants of sapphire (α -Al₂O₃) single crystals. *J Appl Phys* 76(12):8032–8036
- Ho KM, Chan CT, Soukoulis CM, Biswas R, Sigalas M (1994) Photonic band gaps in three dimensions: new layer-by-layer periodic structures. *Solid State Commun* 89(5):413–416
- Huang X (2009) High temperature radiation heat transfer performance of thermal barrier coatings with multiple layered structures. *J Eng Gas Turbines Power* 131(1):011301
- Inan US, Inan AS (2000) *Electromagnetic waves*. Upper Saddle River, New Jersey
- Jackson JD (1998) *Classical electrodynamics*. John Wiley & Sons, Inc, New York
- Joannopoulos JD, Meade RD, Winn JN (1995) *Photonic crystals: molding the flow of light*. Princeton University Press, Princeton
- Johnson S, Joannopoulos J (2001) Block-iterative frequency-domain methods for Maxwell's equations in a planewave basis. *Opt Express* 8(3):173–190
- Kelly MJ, Wolfe DE, Singh J, Eldridge J, Zhu D-M, Miller R (2006) Thermal barrier coatings design with increased reflectivity and lower thermal conductivity for high-temperature turbine applications. *Int J Appl Ceram Technol* 3(2):81–93
- Kim MY, Baek SW (1996) Numerical analysis of conduction, convection, and radiation in a gradually expanding channel. Numerical heat transfer, Part A: applications. *Int J Comput Methodol* 29(7):725–740
- Kittel C (1966) *Introduction to solid state physics*. John Wiley & Sons, Inc, New York
- Ko M, Anand NK (2008) Three-dimensional combined convective-radiative heat transfer over a horizontal backward-facing step—a finite-volume method. Numerical heat transfer, Part A: Applications. *Int J Comput Methodol* 54(2):109–129
- Krishnaprakas CK, Narayana KB, Dutta P (2000) Radiation in boundary layer flow of an absorbing, emitting and anisotropically scattering fluid. *Int J Numer Methods Heat Fluid Flow* 10(5):530–540
- Lee W, Ji R, Gosele U, Nielsch K (2006) Fast fabrication of long-range ordered porous alumina membranes by hard anodization. *Nat Mater* 5(9):741–747
- Leung KM, Liu YF (1990) Full vector wave calculation of photonic band structures in face-centered-cubic dielectric media. *Phys Rev Lett* 65(21):2646
- Liu L, Liu JT (1999) Photonic band structure in the nearly plane wave approximation. *Eur Phys J B Condens Matter Complex Syst* 9(3):381–388
- Mekis A, Chen JC, Kurland I, Fan S, Villeneuve PR, Joannopoulos JD (1996) High transmission through sharp bends in photonic crystal waveguides. *Phys Rev Lett* 77(18):3787
- Modest MF (2003) *Radiative heat transfer*. Boston Academic Press, Amsterdam
- Nicholls JR, Lawson KJ, Johnstone A, Rickerby DS (2002) Methods to reduce the thermal conductivity of EB-PVD TBCs. *Surf Coat Technol* 151–152:383–391
- Niklasson GA, Granqvist CG, Hunderi O (1981) Effective medium models for the optical properties of inhomogeneous materials. *Appl Opt* 20(1):26–30
- Noda S, Imada M, Okano M, Ogawa S, Mochizuki M, Chutinan A (2002) Semiconductor three-dimensional and two-dimensional photonic crystals and devices. *IEEE J Quantum Electron* 38(7):726–735
- Oskooi AF, Zhang L, Avniel Y, Johnson SG (2008) The failure of perfectly matched layers, and towards their redemption by adiabatic absorbers. *Opt Express* 16(15):11376–11392
- Oskooi AF, Roundy D, Ibanescu M, Bermel P, Joannopoulos JD, Johnson SG (2010) Meep: a flexible free-software package for electromagnetic simulations by the FDTD method. *Comput Phys Commun* 181(3):687–702
- Painter O, Lee RK, Scherer A, Yariv A, O'Brien JD, Dapkus PD, Kim I (1999) Two-dimensional photonic band-gap defect mode laser. *Science* 284(5421):1819–1821
- Prather DW, Shi S, Sharkawy A, Murakowski J, Schneider GJ (2009) *Photonic crystals theory, applications, and fabrication*. John Wiley & Sons, Inc, Hoboken
- Robert Siegel JH (2002) *Thermal radiation heat transfer*. Taylor & Francis, New York
- Rolin MN, Soloukhin RI, Yurevich FB (1981) Heat and mass transfer in an emitting compressed layer with reflection from the body surface and injection of ablation products. *Int J Heat Mass Transf* 24(11):1771–1782
- Sahrai M, Aas S, Mahmoudi M (2010) Subluminal to superluminal pulse propagation through one-dimensional photonic crystals

- with a three-level atomic defect layer. *Eur Phys J B Condens Matter Complex Syst* 78(1):51–58
- Shklover V, Braginsky L, Witz G, Mishrikey M, Hafner C (2008) High-temperature photonic structures. thermal barrier coatings, infrared sources and other applications. *J Comput Theor Nanosci* 5:862–893
- Siegel R, Spuckler CM (1998) Analysis of thermal radiation effects on temperatures in turbine engine thermal barrier coatings. *Mater Sci Eng A* 245(2):150–159
- Sözüer HS, Haus JW, Inguva R (1992) Photonic bands: convergence problems with the plane-wave method. *Phys Rev B* 45(24):13962
- Taflove A, Hagness SC (2000) *Computational electrodynamics: the finite-difference time-domain method*. Artech, Norwood
- von Blanckenhagen B, Tonova D, Ullmann J (2002) Application of the Tauc-Lorentz formulation to the interband absorption of optical coating materials. *Appl Opt* 41(16):3137–3141
- Wang D, Huang X, Patnaik P (2006) Design and modeling of multiple layered TBC system with high reflectance. *J Mater Sci* 41(19):6245–6255
- Winn JN, Fink Y, Fan S, Joannopoulos JD (1998) Omnidirectional reflection from a one-dimensional photonic crystal. *Opt Lett* 23(20):1573–1575
- Wolfe DE, Singh J, Miller RA, Eldridge JI, Zhu D-M (2005) Tailored microstructure of EB-PVD 8YSZ thermal barrier coatings with low thermal conductivity and high thermal reflectivity for turbine applications. *Surf Coat Technol* 190(1):132–149
- Yablonovitch E (2001) *Photonic crystals: semiconductors of light*. Scientific American
- Yablonovitch E, Gmitter TJ, Leung KM (1991) Photonic band structure: the face-centered cubic case employing nonspherical atoms. *Phys Rev Lett* 67:2295–2298
- Yang SG, Li T, Huang LS, Tang T, Zhang JR, Gu BX, Du YW, Shi SZ, Lu YN (2003) Stability of anodic aluminum oxide membranes with nanopores. *Phys Lett A* 318(4–5):440–444
- Yeh P (1988) *Optical waves in layered media*. John Wiley & Sons, New York